Journal of Geophysical Research Solid Earth

Supporting Information for

Different formation histories between the African and Pacific large low shear-wave velocity provinces as revealed by their water contents

Xiao-Yan Gu[1], Piao-Yi Wang[2], Eero Hanski[3], Bertrand Moine[4], Takeshi Kuritani[5], Mitsuhiro Nakagawa[5], Qun-Ke Xia[1], Jia Liu[1], Huan Chen[1]

[1]Key Laboratory of Geoscience Big Data and Deep Resource of Zhejiang Province, School of Earth Sciences, Zhejiang University, Hangzhou 310027, China, [2]School of Earth and Space Sciences, University of Science and Technology of China, Hefei 230026, China, [3]Oulu Mining School, University of Oulu, P. O. Box 3000, 90014 Oulu, Finland, [4]Université de Lyon, UJM-Saint-Etienne, UCA, IRD, CNRS, Laboratoire Magmas et Volcans, UMR6524, Saint-Etienne, France, [5]Graduate School of Science, Hokkaido University 060-0810, Japan

Contents of this file

Additional Supporting Information (Files uploaded separately)

Introduction

Supplementary information contains Text S1 to S4, with the geological background and petrological features of studied samples, the details of analytical procedures, the calculation procedures for water contents in primary melts and mantle sources for hotspot-related OIBs, including Kerguelen and Crozet basalts.

Text S1. Geological background and petrological features of studied samples

The samples related to the Kerguelen mantle plume were collected from the Kerguelen Archipelago. The Kerguelen Archipelago, situated in the southeast Indian Ocean, is a subaerial expression of the Kerguelen hotspot with the age of related basalts ranging from ~29 Ma to recent. The petrological and geochemical characteristics display significant divergence between basalts with the age of >25 Ma and <25 Ma in the archipelago. Previous studies proposed that this variation is closely related to the proximity of the plume to the Southeast Indian Ridge (SEIR) and the variable lithospheric thickness. Tholeiitic to transitional basalts older than 25 Ma have more depleted Sr-Nd-Pb-Hf isotopic compositions probably due to contamination by the SEIR MORB source mantle when the plume was close to the SEIR axis. The younger alkalic basalts, mainly emplaced in the eastern and southeastern parts of the archipelago and far away from the SEIR, have more enriched Sr-Nd-Pb-Hf isotopic compositions, reflecting the compositional features of the Kerguelen mantle plume.

Ten samples studied here were collected during several field missions, and all of them are from the eastern and southeastern parts of the Kerguelen Archipelago and have ages of 22-25 Ma (Figure 1). Thin sections show that the samples are mostly fresh and display olivine- and clinopyroxene (Cpx)-phyric to aphyric textures. The olivine and Cpx phenocrysts have model proportions up to 20 vol.% in several samples and large portions of them are euhedral or subhedral (Figure S1).

The geological setting of the Crozet Archipelago has been described in detail by Breton et al. (2013). They analyzed geochemical and Sr-Nd-Pb isotopic compositions of bulk rocks, chemical compositions of olivine and Cpx phenocrysts, and He isotopic compositions of olivine phenocrysts in Cenozoic basalts from three islands (East, Possession, and Penguins Islands) belonging to the Crozet Archipelago. Four samples from the Penguins Island were selected for this study: OVPG8, OVPG9, OVPG13 and OVPG38. Detailed petrographical descriptions can be found in the supplementary text of Breton et al. (2013).

Text S2. Analytical methods

Major and trace element compositions of bulk rocks.

Fresh interior slices of the Kerguelen samples and one Crozet sample OVPG8 were picked and grinded into 200-mesh powders. All analyses were performed at ALS Chemex (Guangzhou, China) Co., Ltd. After heating the powders at 1000 °C for 90 min, the loss on ignition was measured. The contents of major elements were analyzed by X-Ray fluorescence spectrometry on fused glass disks. The precision for major oxides with an abundance of >1 wt.% was 1-3% and for other oxides with an abundance of <1 wt.%, it was approximately 10%. For trace elements, the sample powders were dissolved in an HNO_3-HF-$HClO_4$ mixture held in a high-pressure Teflon bomb. After drying, the solutions were diluted by dilute HNO_3. The final analyses were carried out by a PerkinElmer inductively coupled plasma mass spectrometer (ICP-MS). The precision is better than 5% for most trace elements. The results of bulk-rock major and trace element compositions are shown in Tables S1 and S2, respectively, also including the adopted data from Breton et al. (2013) for other three samples (OVPG9, OVPG13 and OVPG38).

Sr-Nd-Pb isotopic compositions.

Sr, Nd, and Pb isotopic analyses for the Kerguelen samples were conducted using a multi-collector inductively coupled plasma mass spectrometer (MC–ICP–MS; Thermo Fisher Scientific Neptune Plus) at Hokkaido University, Japan. Analytical procedures for chemical separations followed the methods of Pin et al. (1994) and Noguchi et al. (2011) for Sr, Pin et al. (1994) and Pin and Zalduegui (1997) for Nd, and Kuritani and Nakamura (2002) for Pb. The normalizing factors used for internal corrections were $^{86}Sr/^{88}Sr = 0.1194$ for Sr and $^{146}Nd/^{144}Nd = 0.7219$ for Nd. Mass fractionation for Pb was corrected using Tl as an external standard ($^{205}Tl/^{203}Tl = 2.3871$; Dunstan et al., 1980). Additional corrections were then performed by applying a standard bracketing method using NIST987, JNdi-1, and NIST981 for Sr, Nd, and Pb isotopic analyses, respectively, and normalized to $^{87}Sr/^{86}Sr = 0.710214$ for NIST 987, $^{143}Nd/^{144}Nd = 0.512117$ for JNdi-1, and $^{206}Pb/^{204}Pb = 16.9424$, $^{207}Pb/^{204}Pb = 15.5003$, and $^{208}Pb/^{204}Pb = 36.7266$ for NIST981 (Kuritani & Nakamura, 2003). The Sr, Nd, and Pb isotopic ratios of JB-3 (from the Geological Survey of Japan) measured during this study, reference values, and standard deviations for replicate analyses are provided in Table A1 of Kuritani et al. (2020). The results of Sr-Nd-Pb isotopic compositions for the Kerguelen samples are shown in Table S3, also including the adopted data from Breton et al. (2013) for the Crozet samples.

Major element compositions of olivine and Cpx phenocrysts.

Analyses on phenocrysts were performed by a Shimadzu electron probe microanalyzer (EPMA 1720) at the School of Earth Sciences, Zhejiang University (China). A series of natural and synthetic minerals or oxides were used as standards. For every sample, several large olivine and Cpx grains were analyzed from cores to rims to monitor the intra-grain compositional heterogeneity. The operating conditions were set at an accelerating voltage of 15 kV and a beam current of 20 nA with a 5-μm beam size. For Cpx phenocrysts, the analyzed positions were placed within or close to the FTIR analysis spots. The final data were compiled after correction using a program based on the ZAF procedure. Major element compositions of Cpx and olivine are listed in Dataset S1.

Trace element composition of Cpx phenocrysts.

The concentrations of trace elements in Cpx phenocrysts from Kerguelen and Crozet basalts were analyzed at the LA-ICPMS laboratory of Zhejiang University (China). The laser system we used was an Analyte HE (Teledyne CETAC technologies, USA) coupled with a HelEx II two-volume sample chamber. The system was equipped with a Coherent 193 nm ArF-excimer laser (COMPex Pro 102F) with max energy density of 45 J/cm2. The laser was set at 6 Hz and 5 J/cm2 energy per pulse and the ablation times were typical 40 s. Washout time between ablation was 30 s and blank count rates were measured for 20 s prior to ablation. The ablation crater diameters were 60 μm throughout this study. The sample aerosol was carried out with high purity helium. The flow rate of helium was set to 0.6 and 0.3 L/min for the cell and arm of HelEx II sample chamber. The helium carrier gas was homogenized with 'Squid' smoothing interface before mixed with nebulizer argon flow, and then was introduced into ICPMS. The ICPMS used was an iCAP RQ (Thermofisher, USA) with parameters set at: 14L/min plasma cool flow, 0.8 L/min auxiliary flow, 0.9 L/min nebulizer flow, 1500 W RF power, 10 ms dwell time per isotope. The mass spectrometer was tuned to give maximum, stable signals at low oxide formation (ThO/Th < 1%) with autotune performed on NIST SRM 612. Standards were measured before and after 5-8 spot analyses of samples. The results of the sample analyses were processed with the ICPMSDataCal software (Liu et al., 2008). The signal intensities (counts per ppm) for each element were calibrated against the NIST SRM 610 silicate glass, and the Ca content of the Cpx analyzed by the electron microprobe was used as an internal standard. The NITS SRM 612 (every 6 spot analyses), BHVO-2, BCR-2 and MPI-DING glass were measured as unknown. Typical analytical precisions ranged from 2% to 5%.

Water contents in Cpx and olivine phenocrysts.

Unpolarized IR spectra of Cpx and olivine phenocrysts were acquired on double-polished thin sections 0.075-0.195 mm in thickness, using a Nicolet iS50 FTIR attached to a Continuμm microscope equipped with a liquid nitrogen cooled MCT-A detector and a KBr beam splitter at the School of Earth Sciences, Zhejiang University (China). During the analysis, the entire instrument was flushed by a continuous dry air flow. Spectra in the wavenumber range of 1000 to 5500 cm^{-1} were collected in the optically clean, inclusion- and crack-free areas using square apertures (30×30 to 100×100 μm^2) adjusted according to the grain size and quality. The sizes of analyzed Cpx and olivine phenocrysts range from tens of micrometers to >1 mm (along the major axis). 128 scans at a resolution of 4 cm^{-1} were accumulated for every spectrum. Several representative spectra of Cpx and olivine are shown in Figure S4a and b, respectively. The water contents were calculated from IR spectra based on the modified Beer-Lambert law:

$$C_{H_2O} = 3A/\varepsilon t \quad (1)$$

in which C_{H_2O} is the water content (wt.ppm), A is the integrated absorbance (cm^{-2}), ε is the molar absorption coefficient (7.09 $ppm^{-1}cm^{-2}$ for Cpx from Bell et al., 1995; 5.32 $ppm^{-1}cm^{-2}$ for olivine from Bell and Rossman, 2003), and t is the thickness of thin section (in cm). Calculated water contents in Cpx and olivine phenocrysts are shown in Dataset S1.

Text S3. Water contents in melts

Calculation of water contents in melts equilibrated with Cpx phenocrysts.

The procedure established by Xia et al. (2013) was followed to retrieve water contents in the melts equilibrated with Kerguelen and Crozet basalts. The H_2O partition coefficient between Cpx and melt ($D_{H_2O}^{Cpx/melt}$) was calculated on the basis of the major element data of Cpx phenocrysts using the following equation from O'Leary et al. (2010):

$$\ln D_{H_2O}^{Cpx/melt} = -4.2(\pm 0.2) + 6.5(\pm 0.5)X_{Al^{IV}}^{Cpx} - 1.0(\pm 0.2)X_{Ca}^{Cpx} \quad (2)$$

where $X_{Al^{IV}}^{Cpx}$ and X_{Ca}^{Cpx} are the molar fractions of tetrahedrally coordinated Al and Ca cations, respectively, calculated on the basis of six oxygen atoms per formula unit of Cpx. The water contents in the melts were calculated from the water contents of Cpx phenocrysts by dividing them by $D_{H_2O}^{Cpx/melt}$.

According to the calculation procedure, the water content of a Cpx phenocryst can be determined by analyzing an unoriented grain under unpolarized radiation by means of FTIR. Theoretical calculations and experimental tests have confirmed that this approach gives a reliable water content estimate for a single Cpx phenocryst within a 20% difference from the result based on the polarized IR spectrum (obtained by polarized IR light focused on an oriented grain), when the unpolarized IR spectrum of the Cpx phenocryst has three groups of OH bands (at ~3640 cm^{-1}, ~3520 cm^{-1} and ~3460 cm^{-1}) and the height of all the peaks being <0.3 (Xia et al., 2013). Taking all the uncertainties in this procedure into consideration (caused by the absorption coefficient, the thickness measurement, the unpolarized measurement, and the partition coefficient calculation), the total uncertainty in the calculated water content of the melt is not more than 32% (Liu et al., 2015). Calculated water contents in melts equilibrated with Cpx phenocrysts are shown in Dataset S1 along with major element compositions of Cpx phenocrysts.

Estimation of water contents in primary melts of basalts

Kerguelen and Crozet basalts

We only took into consideration the melt water contents estimated by Cpx phenocrysts with Mg# higher than 85 in samples EF92-25 and OVPG38, which have preserved their initial water contents, in order to decrease the error during the estimation of water contents in primary melts of the Kerguelen and Crozet basalts, respectively. These samples have experienced olivine/Cpx accumulation, which is responsible for too high Mg# of bulk rocks to be in equilibrium with Mg#

of olivine and Cpx. To retrieve the compositions of primary melts for such basalts, we made inverse estimation by stepwise extraction of equilibrated olivines from bulk-rock compositions until the melts reached Fe-Mg exchange equilibrium with analyzed olivine phenocrysts of highest Mg# in the samples. Here, we assumed that only olivine accumulation or fractional crystallization is the reason for the deviation of the bulk rocks from the compositions of their corresponding primary melts. Then, the proportions of added olivine were calculated to obtain the compositions of primary melts until equilibrated olivines have Mg# = 90. The relationship among the contents of major elements and petrographic observations indicate that many of studied samples have experienced olivine/Cpx accumulation to cause high MgO contents in bulk rocks (>12 wt.%). We use the bulk compositions after eliminating the effects of crystal accumulation as the initial melt compositions of olivine addition calculation for the primary melt compositions. With the assumption of complete incompatibility of H_2O in olivine in basaltic melts, the water contents in primary melts of the Kerguelen and Crozet basalts were back calculated by adding the same amount of olivine to the melt diluting the water contents estimated by Cpx phenocrysts.

Compilation of water content data for hotspot-related OIBs from literature

The references for basalts from different ocean islands are listed in the caption of Figure 4. There are no previous studied on basalts from some typical hotspots for water contents (e.g., Tristan and Gough). We compiled H_2O abundance data previously reported for OIBs related to many hotspots, which overlie mantle plumes explicitly evidenced by geophysical observations and are geographically associated with the two LLSVPs (Dataset S2). Some melt inclusions and basaltic glasses which have been reported to have experienced degassing or diffusive water loss were not taken into consideration. For example, some melt inclusions from Azores and Canary hotspots have lost part of their initial water, these results have been excluded, and only the results of melt inclusions preserving initial water contents were considered for the data compilation (Azores, Métrich et al. (2014); Canary, Longpré et al. (2017)). Walowski et al. (2019) have also measured water contents in melt inclusions from La Palma Island (Canary). But these melt inclusions may have experienced water loss in diverse degrees by degassing and no strong evidence supported the preservation of initial water contents in them (Walowski et al., 2019). Thus, these data for the Canary hotspot are not considered for the data compilation. In order to further construct the water contents of individual primary melts and make comparison of H_2O/Ce ratios, we only compiled water content data reported along with the major element compositions and Ce concentrations in melts.

Estimation of water contents in primary melts of OIBs

From the compilation of water contents in these OIBs, it is noteworthy that many melt inclusions and basaltic glasses of OIBs investigated for water contents in previous studies have relatively low MgO contents (mostly lower than 8 wt.%; Figure 4a) and a broad negative correlation between H_2O and MgO (Figure 4a) indicates that crystallization differentiation processes have modified the water inventory in these melts. In order to make a comparison between the water contents among OIBs, we calculated water contents in individual primary melts after adding olivine incrementally to melts to obtain primary melt compositions. With melt evolution, other crystallization phases (Cpx, plagioclase, and Fe-Ti oxides) emerge, so we have merely considered the compositions and water contents of melt inclusions and basaltic glasses with highest MgO contents when estimating the compositions and water contents of primary melts by incremental olivine addition. As H_2O have similar compatibility to Ce and H_2O/Ce ratios should not vary during the differentiation of magmas, we use the average H_2O/Ce ratios for all the melt inclusions or glasses (preserving initial information) in our referenced literatures to represent the H_2O/Ce ratios of corresponding primary melts. The estimated H_2O contents and H_2O/Ce ratios in primary melts of global OIBs, including the Kerguelen and Crozet basalts in this study, are shown in Table 1.

Text S4. Estimation of water contents in mantle sources of OIBs

After obtaining the water contents in the primary magmas, the water contents in the source mantle of basalts can be estimated by partial melting models. Both batch and fractional partial melting models were applied using the following equations (Shaw, 1970):

Batch partial melting: $$C_0^{H_2O} = C_L^{H_2O}\left(D_{H_2O} + F\left(1 - D_{H_2O}\right)\right) \quad (3)$$

Fractional partial melting: $$C_0^{H_2O} = C_L^{H_2O} D_{H_2O}/(1-(1-F)^{\frac{1}{D_{H_2O}}}) \quad (4)$$

In these two equations, $C_0^{H_2O}$ is the water content in the source, $C_L^{H_2O}$ is the water content in the primary melt, D_{H_2O} is the partition coefficient of water between the source rock and melt, and F is the degree of partial melting. For D_{H_2O} between peridotite and basaltic melt, we used partition coefficient value of 0.0085 (melting depth at ~80 km), as experimentally determined by Hirschmann et al. (2009), and the degree of partial melting was set at 5% for alkali OIBs, and 10% for tholeiitic OIBs. The calculation by two melting models generated comparable source water contents for basalts from a given location. The results are reported in Table 1.

As water have distinct partition coefficients between individual mineral phases and melt, D_{H_2O} may change depending on the source lithology. The contribution of pyroxenite in the sources of many hotspots-related OIBs has been repeatedly proposed in previous studies. Assuming that the source lithology of the OIB is composed of 30% garnet pyroxenite (95% Cpx/orthopyroxene + 5% garnet) and 70% peridotite (Sobolev et al., 2007), we calculate D_{H_2O} of 0.011 (melting depth at ~80 km; the calculation process referring to Hirschmann et al. (2009)). In fact, the change of partition coefficient, considering the incorporation of pyroxenite in the sources, does not seem to induce large variations of calculated source water contents of OIBs (Table 1).

Additionally, Hirschmann et al. (2009) observed that D_{H_2O} between peridotite and basaltic melt increases to the maximum value of 0.0085 when melting at depth of ~80 km and decreases with increasing depths. However, it diminishes more slowly in greater depths. We also calculate the source water contents of OIBs applied D_{H_2O} at 0.0046 (melting depth at 150 km) between peridotite and basaltic melt for comparison (Table 1). It can be noted that there is no large variation in the calculated source water contents applying D_{H_2O} of 0.0085 or 0.0046 (not higher than 10%; Table 1).

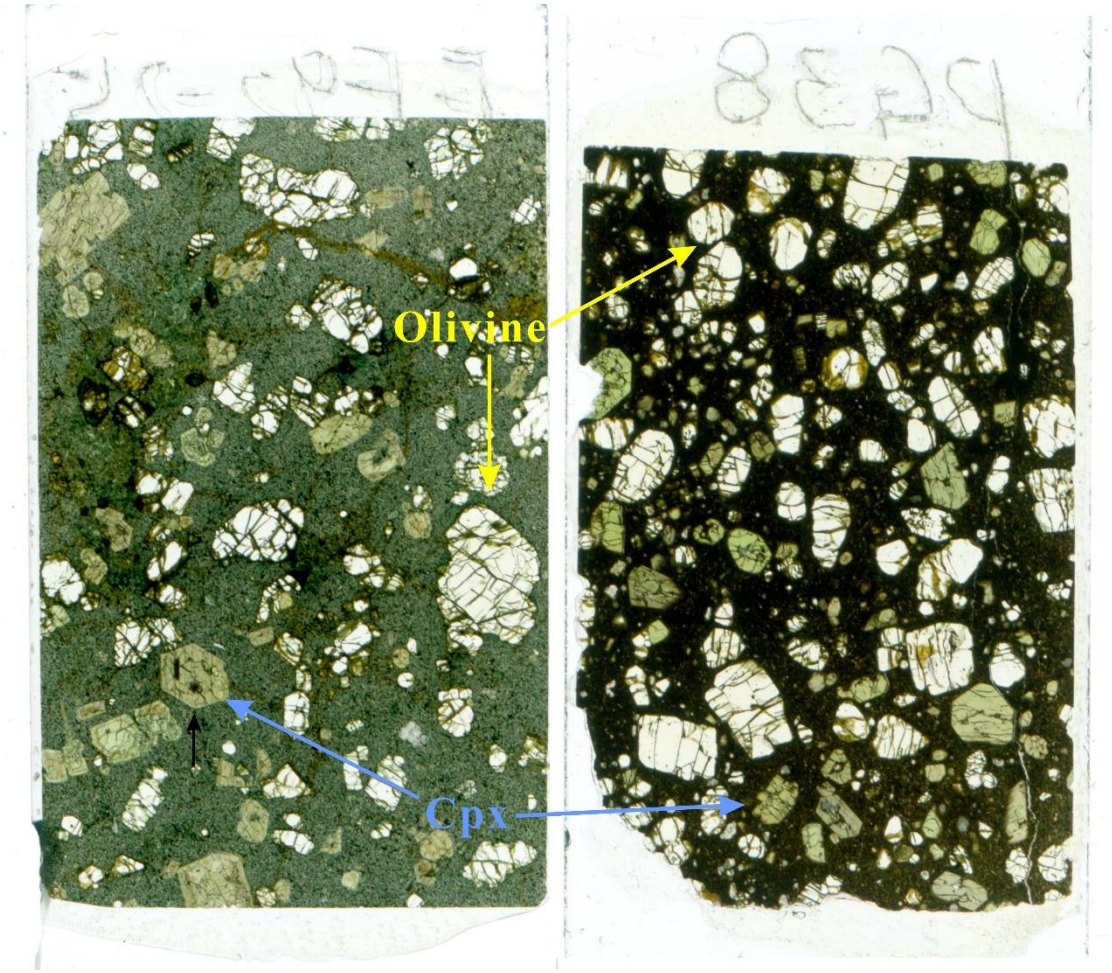

Figure S1 Scanned thin sections of two representative samples, EF92-25 and OVPG38, from the Kerguelen and Crozet Archipelagos, respectively. Both samples display a porphyritic texture with phenocrysts of olivine and clinopyroxene (Cpx).

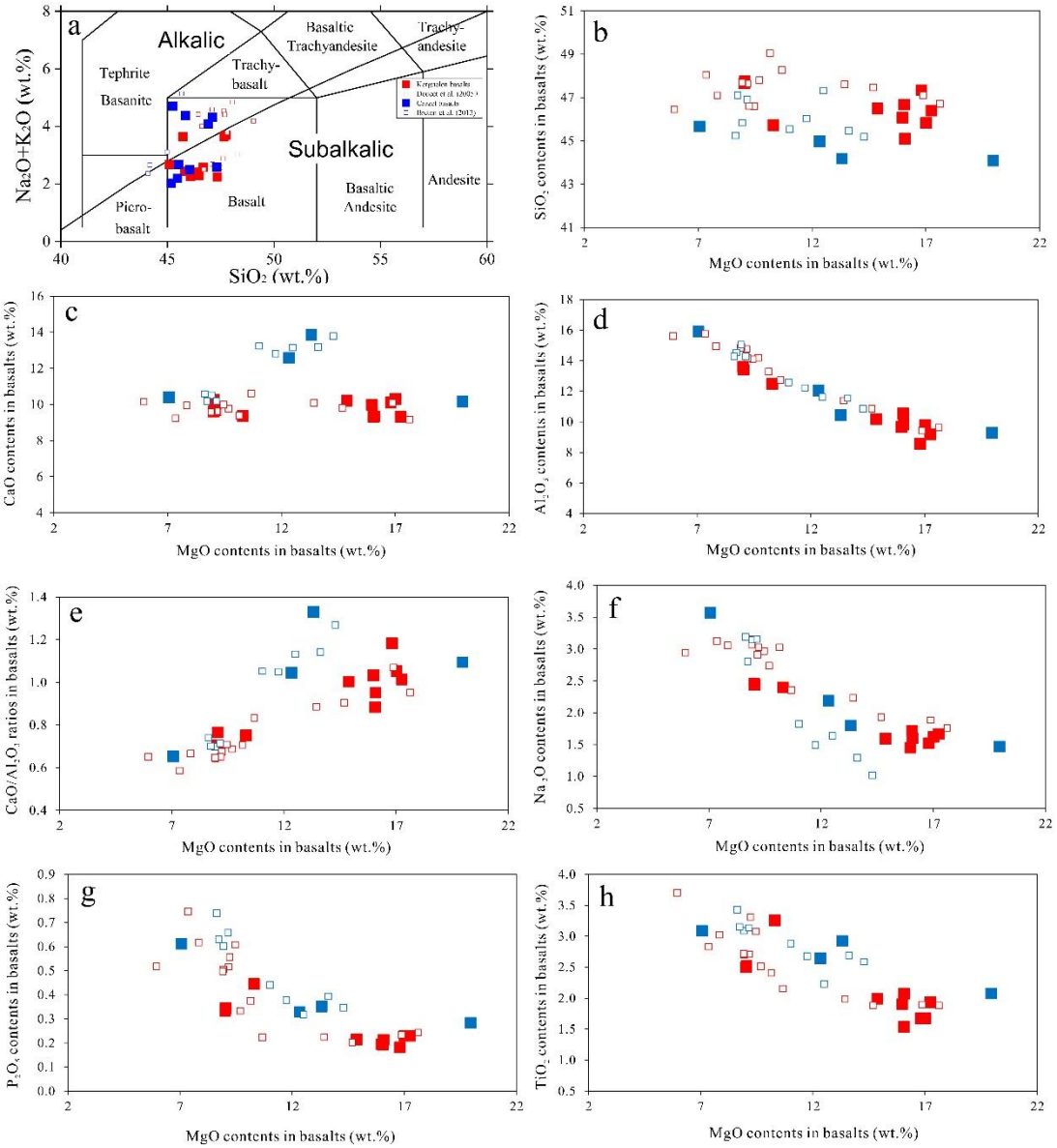

Figure S2 Total alkali versus SiO_2 diagram (a) and plots of selected major element oxides against MgO (b-h) for Kerguelen and Crozet basalts. The small empty squares in red and blue colors represent basalts from the Kerguelen Archipelago (Doucet et al., 2005) and from East and Possession Islands in the Crozet Archipelago (Breton et al., 2013), respectively.

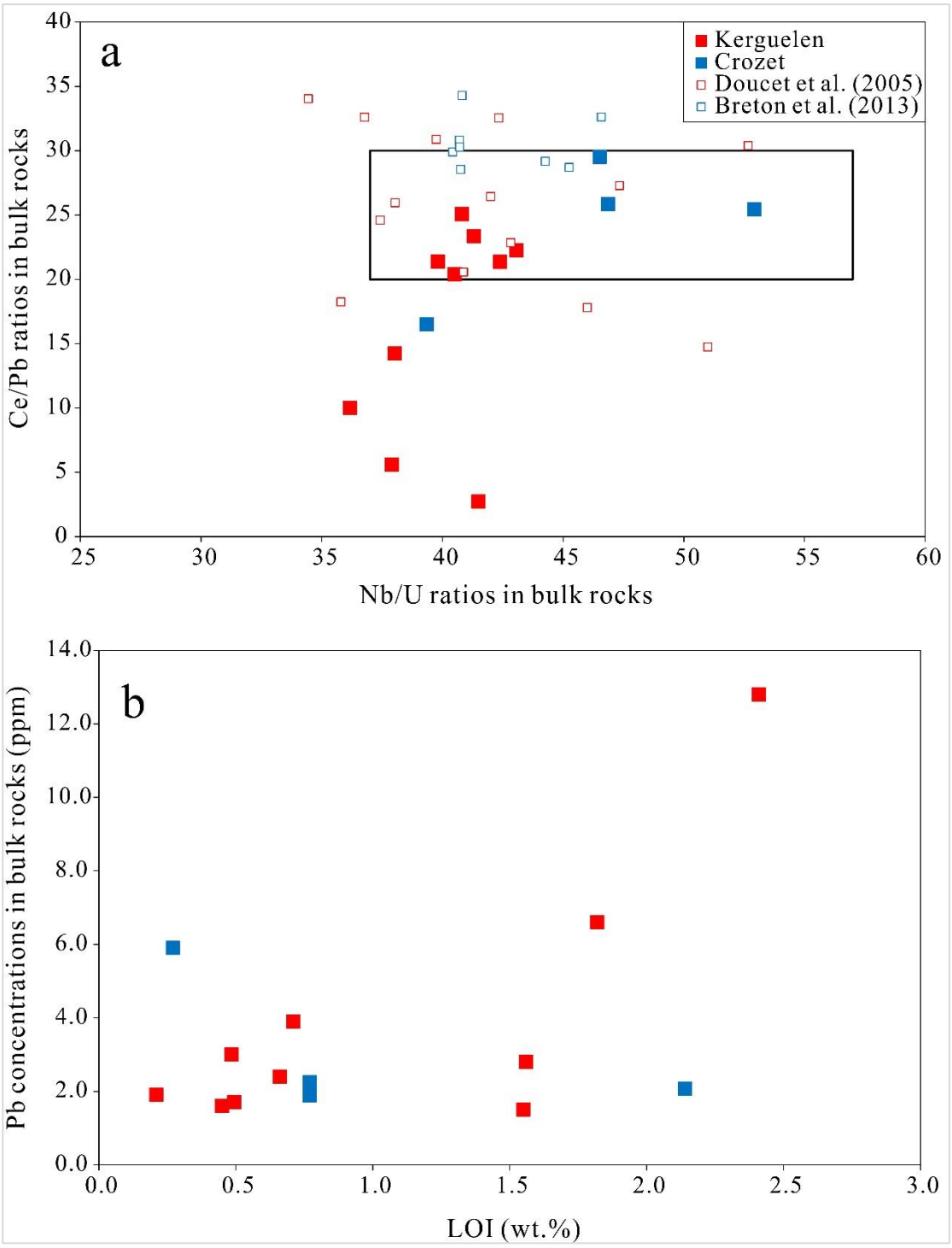

Figure S3 Ce/Pb vs. Nb/U (a), and Pb vs LOI (b) diagrams for bulk-rock samples of Kerguelen and Crozet basalts. The samples with extremely low Ce/Pb ratios have high Pb concentrations and LOI values, meaning that the low Ce/Pb ratios may have been caused by surficial alteration. The data of basalts from the Kerguelen Archipelago (Doucet et al., 2005) and from East and Possession Islands in the Crozet Archipelago (Breton et al., 2013) are also included in (a). The field of Nb/U and Ce/Pb ratios in global OIBs and MORBs (after to Hofmann et al., 1986) is shown by a black rectangle in (a).

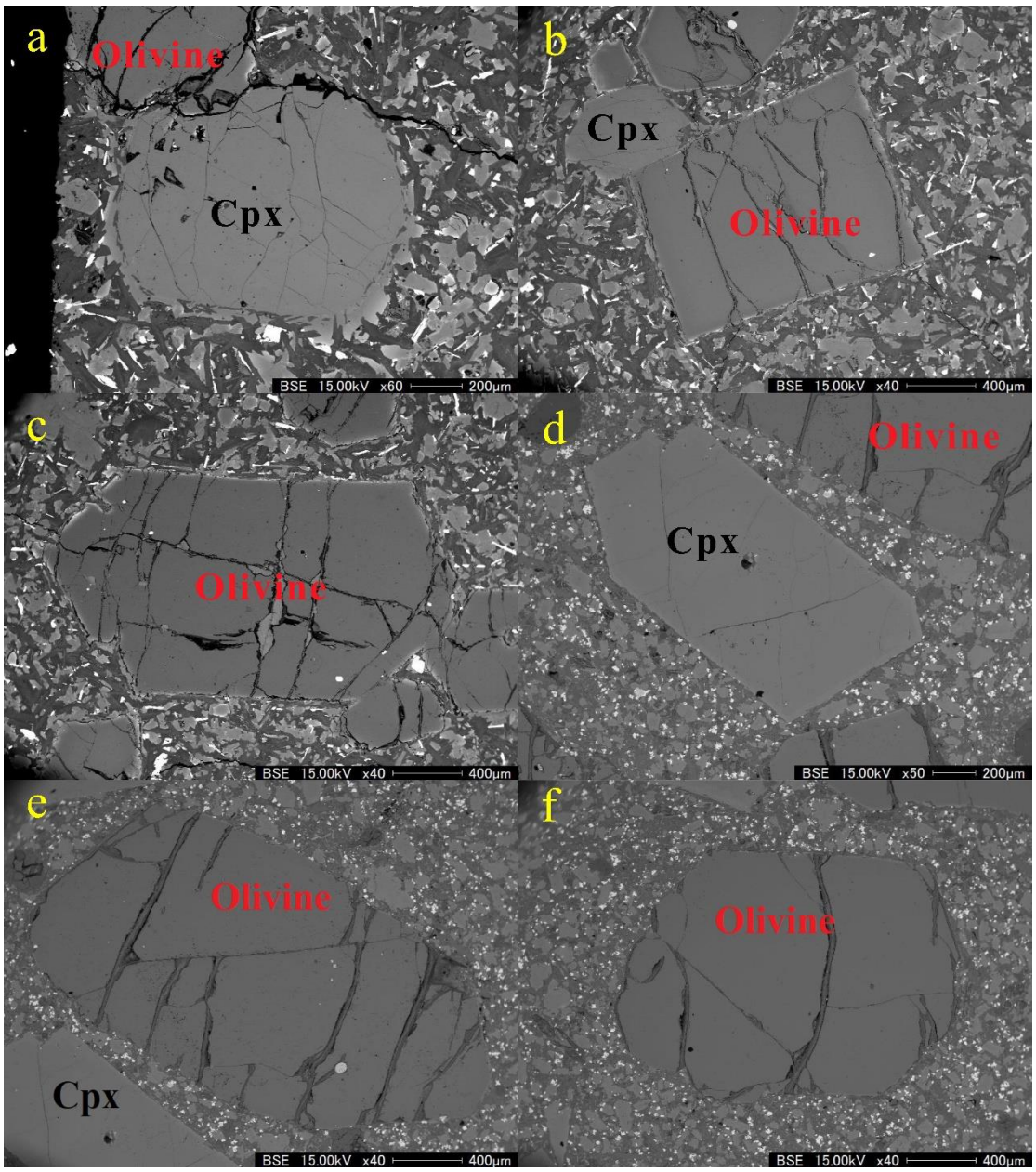

Figure S4 Backscattered electron images of olivine and Cpx phenocrysts in Kerguelen basalt EF92-25 (a-c) and Crozet basalt OVPG38 (d-f).

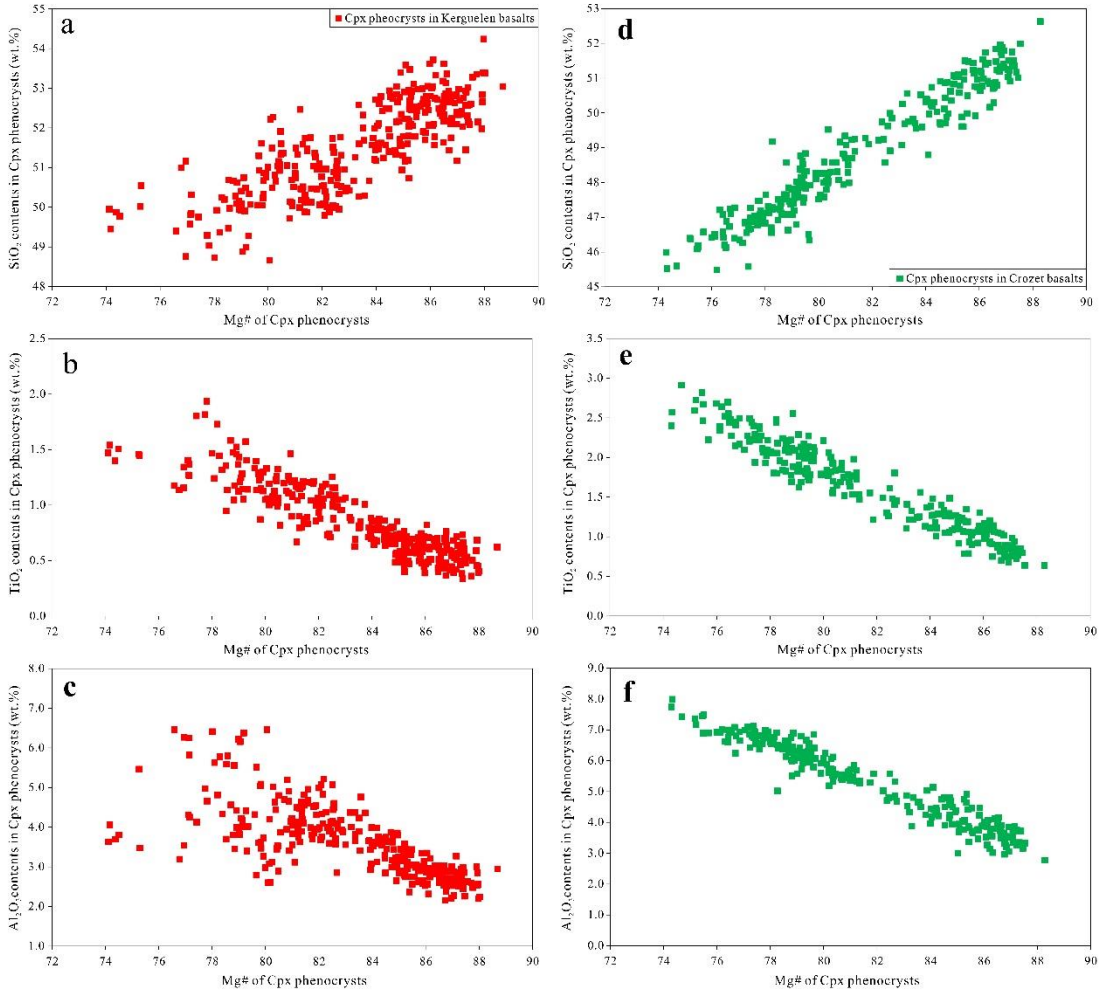

Figure S5 The co-variation of SiO_2, TiO_2 and Al_2O_3 contents with Mg# in Cpx phenocrysts from the studied Kerguelen and Crozet basalts.

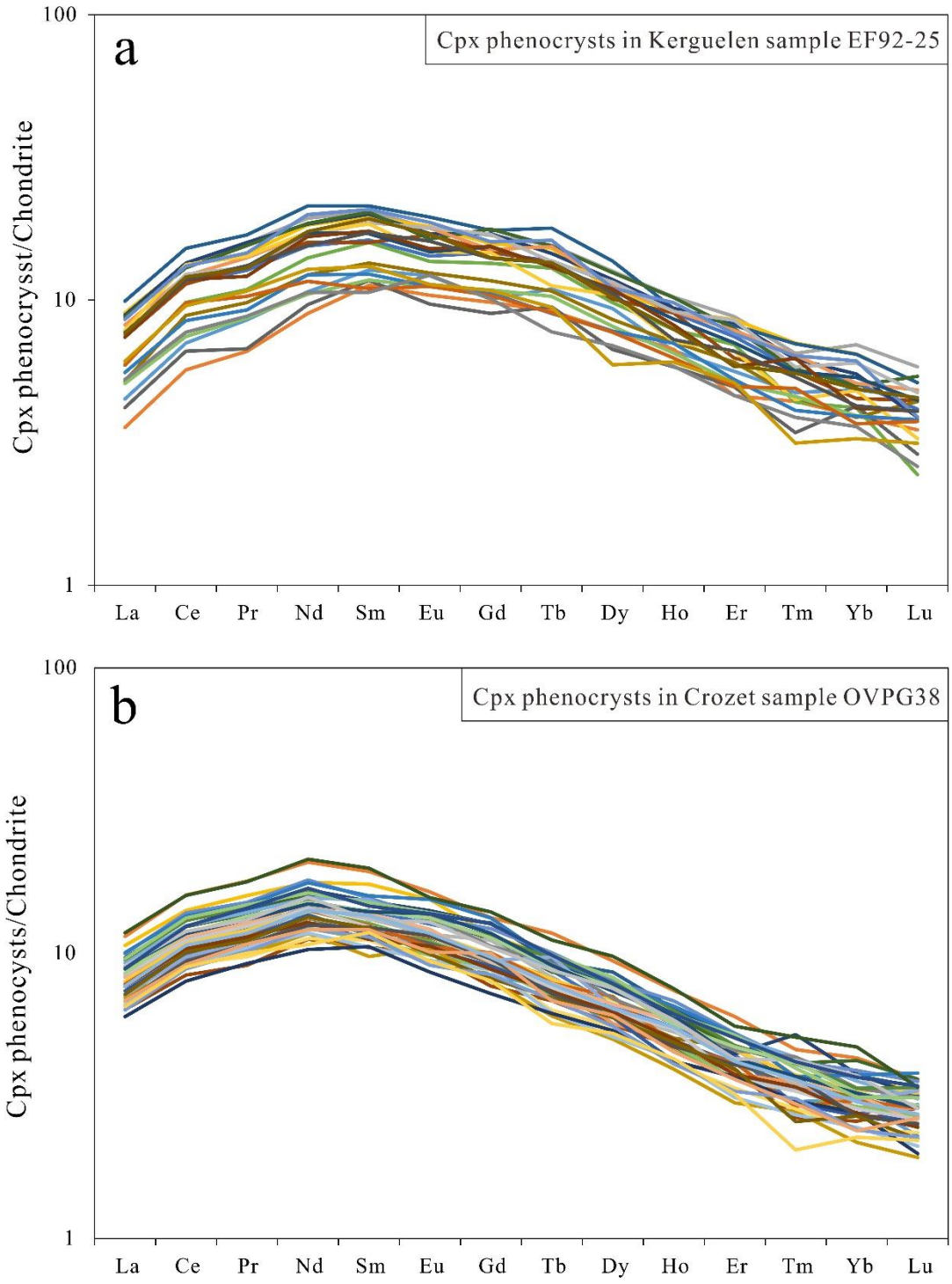

Figure S6 Chondrite-normalized REE pattern of Cpx phenocrysts in representative samples from Kerguelen and Crozet hotspots, EF92-25 (a) and OVPG38 (b), respectively. Normalization values after McDonough and Sun (1995).

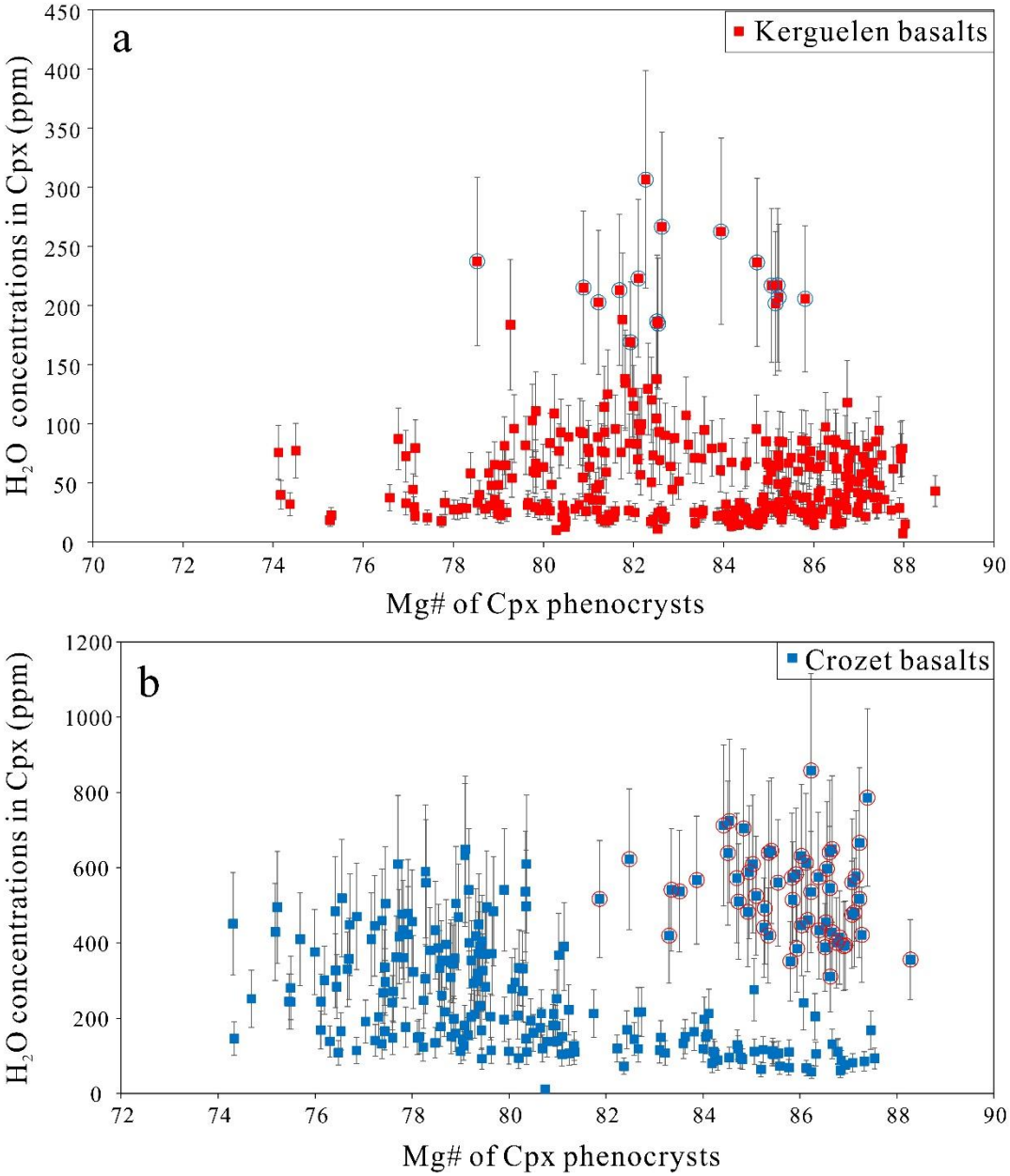

Figure S7 Whole dataset of water contents plotted against Mg# of Cpx phenocrysts from the studied Kerguelen and Crozet basalts. The circled symbols represent Cpx phenocrysts which have preserved their initial water contents, as discussed in the main text. The errors in the water contents were estimated to be 30% due to the use of unpolarized FTIR to measure water contents.

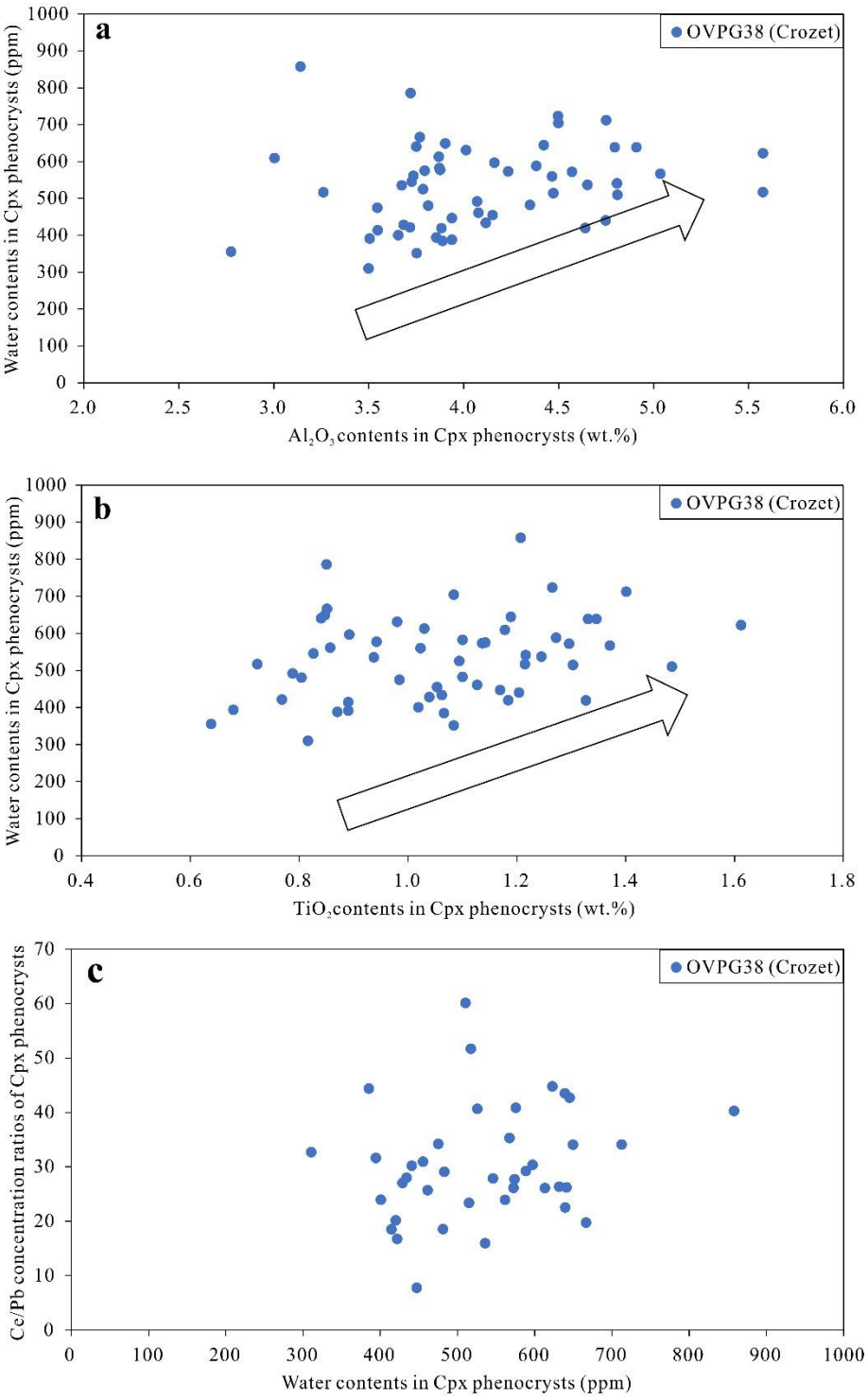

Figure S8 H_2O contents as a function of Al_2O_3 (a) and TiO_2 (b) contents, and Ce/Pb ratios in Cpx phenocrysts from sample OVPG38 (Crozet). The weakly positive correlation of H_2O with Al_2O_3 and TiO_2 indicate that Cpx phenocrysts have preserved their initial H_2O contents. The lack of co-variation between H_2O contents and Ce/Pb ratios suggests that the high water contents in Cpx phenocrysts from sample OVPG38 have not caused by exotic fluid/melt related to the altered oceanic crust.

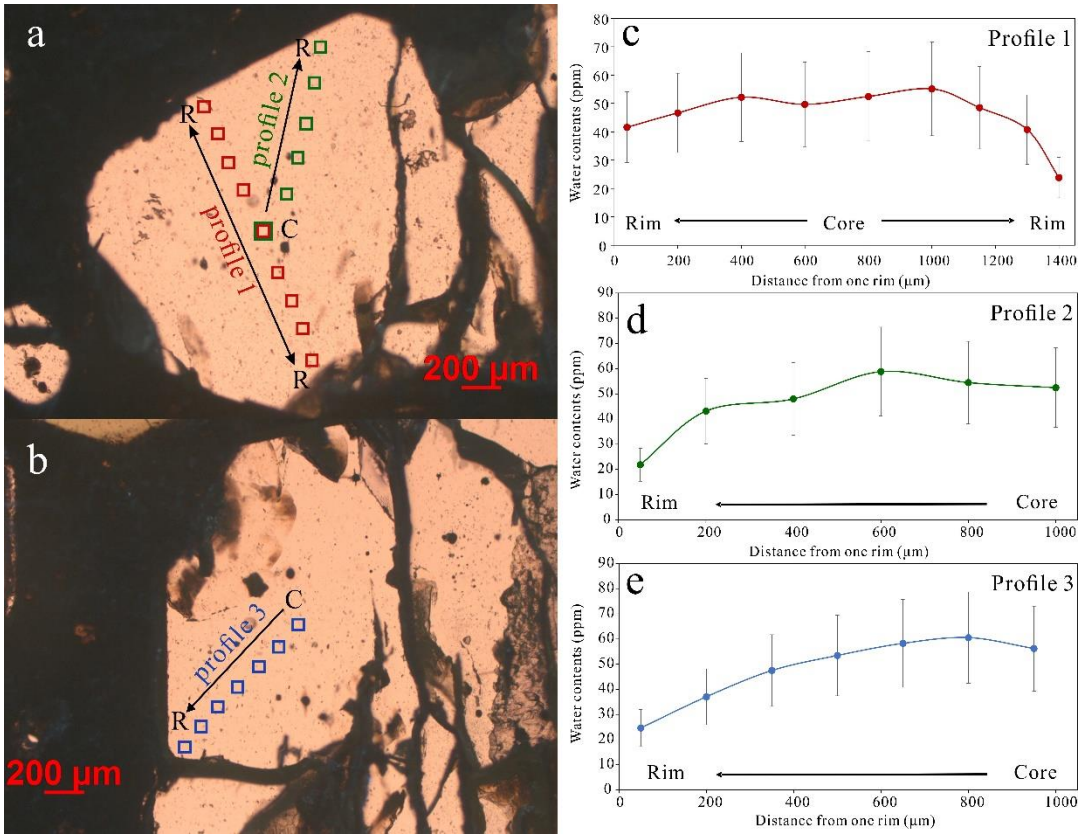

Figure S9 Representative IR profile measurements on two olivine phenocrysts from Crozet basalts. a, b Locations of the core-to-rim (C-R) profiles analyzed on two olivine grains. The step lengths are 200 μm for profiles 1 and 2 and 150 μm for profile 3. **c, d, e Core-to-rim variations of calculated water contents in three profiles.** The water contents show a decrease when approaching the grain rims.

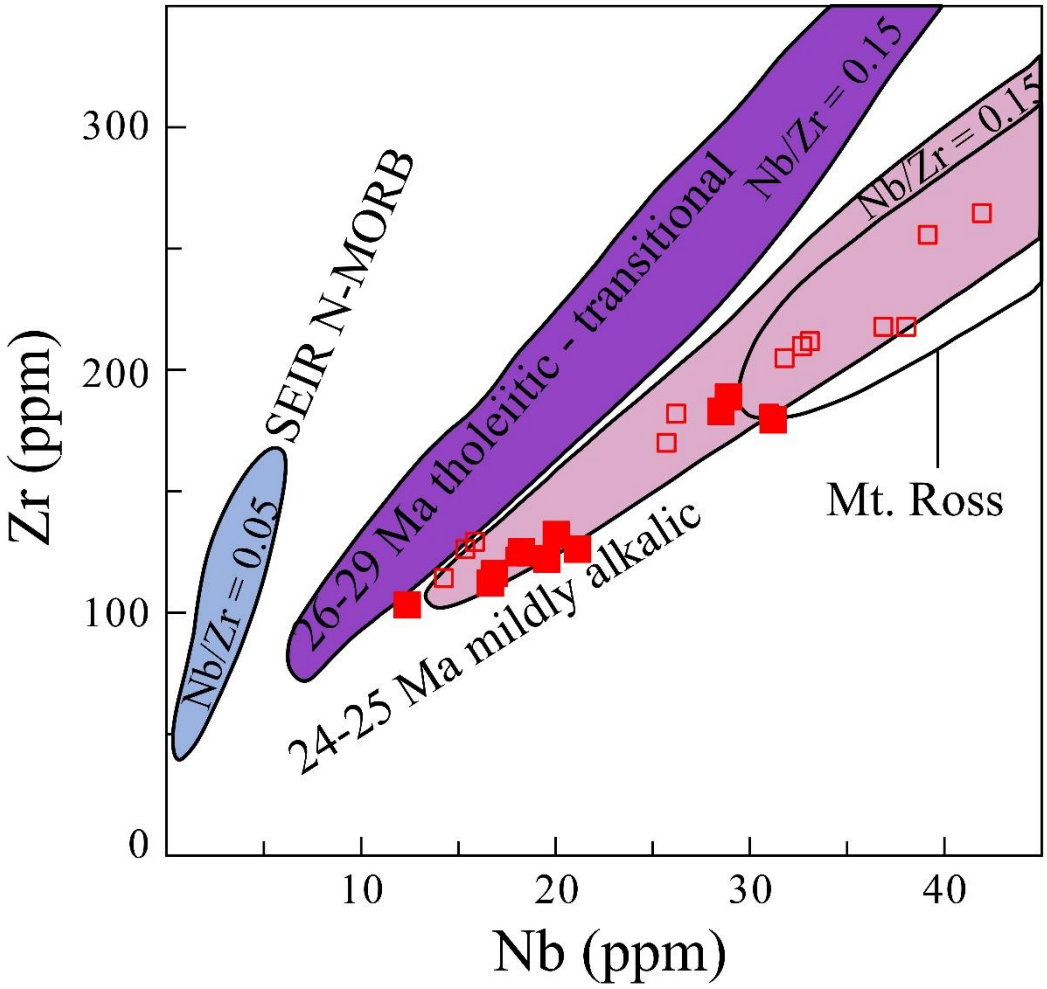

Figure S10 Nb and Zr concentrations in bulk-rock samples of basalts from the Kerguelen Archipelago. The different fields are adopted from Doucet et al. (2005). Basalts dated from 26 to 29 Ma fall between the SEIR N-MORB and basalts with an age younger of 24-25 Ma. The former have been proposed to manifest contamination with SEIR MORB and the latter represent unmodified melting products of the Kerguelen mantle plume. Our samples (solid red symbols) fall in the field defined by the 24-25 Ma basalts. The open squares represent basalts studied by Doucet et al. (2005).

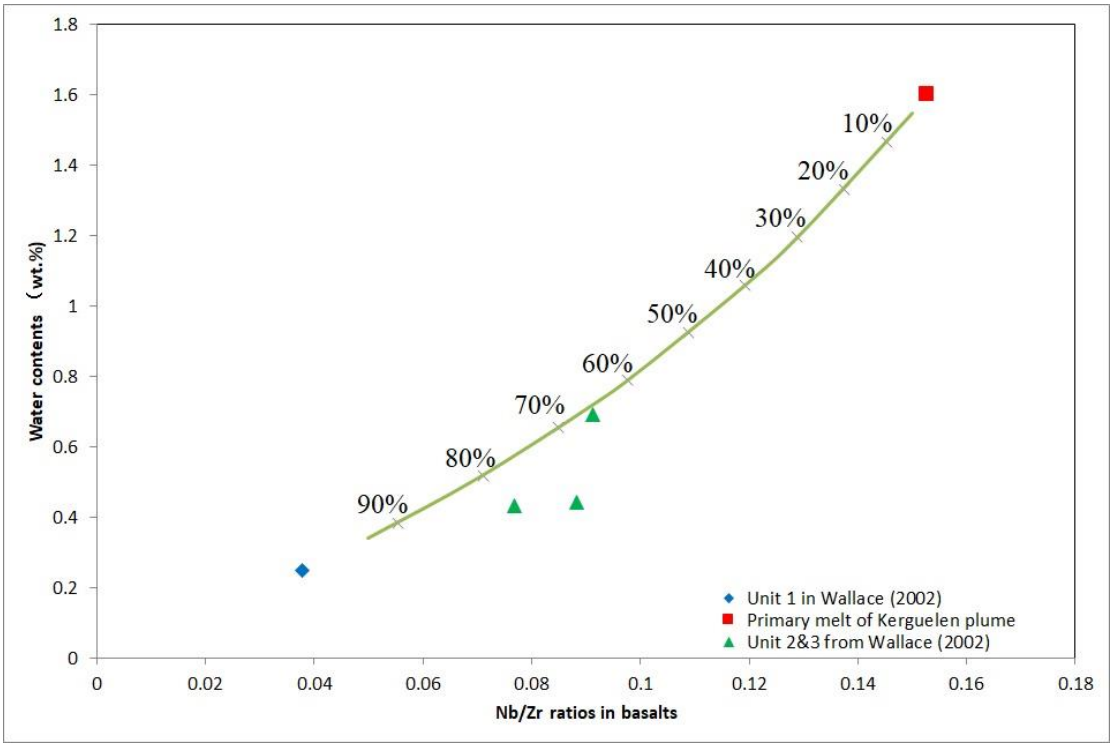

Figure S11 Mixing modeling of the water contents and Nb/Zr ratios in enriched glass units from the NKP (Wallace, 2002). The water content in the primary melt of the Kerguelen plume is based on this study. The unit 1 studied by Wallace (2002) has geochemical signatures similar to those of SEIR MORB (Weis & Frey, 2002). The mixing model follows that of Langmuir et al. (1978), and the percentages by the mixing line represent the proportions of the MORB component. The obtained extents of mixing for glass units 2 and 3, which were used for water content calculations in this study are similar to those estimated from isotopic compositions (Weis & Frey, 2002). This implies that the water content in the primary melt of the Kerguelen plume estimated in this study is reliable.

Kerguelen													
	SiO_2	TiO_2	Al_2O_3	Cr_2O_3	FeO	MnO	MgO	CaO	Na_2O	K_2O	P_2O_5	LOI *	Mg# §
OB93-525	47.76	2.52	13.40	0.05	11.44	0.18	9.04	10.26	2.44	1.25	0.34	0.66	61.03
OB93-526	47.65	2.50	13.60	0.05	12.01	0.19	9.02	9.61	2.46	1.18	0.33	0.71	59.80
CT02-16	45.72	3.25	12.48	0.04	13.08	0.18	10.30	9.36	2.39	1.24	0.44	0.48	60.94
CT02-373	46.07	1.90	9.66	0.13	12.19	0.18	15.99	9.98	1.45	0.81	0.19	2.41	72.21
CT02-376	46.49	1.99	10.18	0.13	12.05	0.18	14.88	10.21	1.60	0.70	0.21	1.82	70.99
CT02-548	47.34	1.67	8.56	0.20	11.41	0.18	16.81	10.12	1.52	0.72	0.18	0.49	74.49
CT02-598	45.10	2.07	9.81	0.11	12.93	0.18	16.08	9.34	1.60	1.08	0.21	1.55	71.12
EF92-18	45.82	1.67	9.79	0.16	11.13	0.17	17.02	10.30	1.62	0.82	0.23	0.21	75.19
EF92-25	46.67	1.54	10.54	0.14	11.49	0.17	16.06	9.31	1.72	0.86	0.19	1.56	73.47
LVLK-85	46.39	1.93	9.19	0.13	11.63	0.17	17.25	9.31	1.67	0.76	0.23	0.45	74.61
Crozet													
OVPG8	45.66	3.09	15.90		11.90	0.21	7.06	10.39	3.57	1.58	0.61	0.27	54.03
OVPG9 ¥	44.18	2.92	10.42		12.11	0.18	13.32	13.87	1.80	0.86	0.35	0.77	68.54
OVPG13	44.98	2.65	12.04		11.79	0.18	12.34	12.57	2.18	0.92	0.33	0.77	67.45
OVPG38	44.09	2.08	9.29		11.58	0.19	19.97	10.16	1.47	0.90	0.28	2.14	77.35

Table S1 Major element compositions of bulk-rock samples of Kerguelen and Crozet basalts in this study. Notes: * LOI=loss on ignition estimated by heating sample powders at 1000 ℃ for 90 min. § Mg# was calculated assuming Fe3+/ΣFe = 0.1. ¥ Compositions of samples OVPG9, OVPG 13 and OVPG38 are adopted from Breton et al. (2013).

	Rb	Ba	Th	U	K *	Nb	Ta	La	Ce	Pb	Pr	Sr	Nd	Zr	Hf	Sm	Eu	Ti *	Gd	Tb	Dy	Ho	Y	Er	Tm	Yb	Lu
Kerguelen																											
OB93-525	29.5	279	3.43	0.69	1.01	28.5	1.9	27.4	56.0	2.4	7.1	434	28.1	183	4.8	6.2	2.0	1.47	5.7	0.9	4.9	0.9	23.2	2.6	0.3	2.0	0.3
OB93-526	27.6	273	3.26	0.76	0.95	28.9	1.9	27.0	55.6	3.9	7.0	399	27.7	189	4.7	6.2	2.2	1.43	5.9	0.9	4.9	1.0	24.5	2.5	0.4	2.1	0.3
CT02-16	34.9	344	3.58	0.77	1.02	31.2	1.9	29.3	61.2	3.0	7.9	695	31.6	180	4.8	6.6	2.5	1.89	6.4	0.9	4.9	0.9	23.2	2.2	0.3	1.8	0.3
CT02-373	17.2	620	1.91	0.40	0.63	16.6	1.3	16.8	34.8	12.8	4.4	804	18.7	112	3.0	4.4	1.5	1.07	4.1	0.7	3.6	0.7	17.1	1.9	0.3	1.5	0.2
CT02-376	15.8	153	2.00	0.48	0.57	18.2	1.3	17.2	36.9	6.6	4.7	253	19.5	125	3.2	4.6	1.5	1.17	4.5	0.7	3.7	0.7	18.4	1.8	0.3	1.5	0.2
CT02-548	17.8	174	2.14	0.46	0.61	19.5	1.1	17.9	36.3	1.7	4.9	272	18.8	122	3.2	4.3	1.4	0.99	4.1	0.6	3.6	0.7	17.8	1.7	0.2	1.4	0.2
CT02-598	23.8	153	1.75	0.39	0.89	16.8	1.3	15.8	33.4	1.5	4.3	628	18.4	116	3.1	4.3	1.5	1.24	4.1	0.6	3.5	0.7	16.6	1.7	0.2	1.4	0.2
EF92-18	18.9	179	2.51	0.53	0.68	21.1	1.4	19.9	40.6	1.9	5.2	340	20.4	126	3.3	4.5	1.5	1.03	4.2	0.6	3.2	0.6	15.0	1.6	0.2	1.2	0.2
EF92-25	34.3	152	1.48	0.34	0.72	12.3	0.9	13.0	28.0	2.8	3.6	343	15.4	103	2.7	3.7	1.3	0.91	3.7	0.6	3.5	0.7	15.2	1.7	0.2	1.3	0.2
LVLK-85	17.9	183	2.23	0.49	0.64	20.0	1.4	19.2	40.1	1.6	4.8	273	20.1	132	3.4	4.5	1.5	1.17	4.6	0.7	3.8	0.8	18.1	1.9	0.3	1.5	0.2
Crozet																											
OVPG8	37.3	403	5.15	1.39	1.55	54.7	3.4	48.0	97.4	5.9	12.2	700	48.5	287	6.6	9.6	3.0	3.03	8.2	1.2	6.6	1.2	31.0	3.2	0.4	2.6	0.4
OVPG9 [§]	21.5	256	2.84	0.69	0.83	32.1	1.7	26.1	55.8	1.9	6.9	441	29.1	175	4.8	6.5	2.1	2.83	5.8		4.5	0.8	21.2	2.0		1.6	0.2
OVPG13	19.6	296	2.95	0.65	0.90	34.4	1.8	27.9	57.0	2.2	7.0	422	28.8	165	4.4	6.2	2.0	2.58	5.6		4.5	0.8	22.7	2.2		1.8	0.3
OVPG38	20.0	218	2.69	0.67	0.86	31.4	1.8	28.0	53.5	2.1	7.0	562	28.7	149	3.7	5.8	1.8	1.98	5.3		4.2	0.8	23.6	2.0		1.6	0.2

Table S2 Trace element compositions of bulk rocks for Kerguelen and Crozet basalts in this study. Note: * K and Ti are shown in wt. % and other elements in ppm. § The compositional data for samples OVPG9, Compositions of OVPG13 and OVPG38 adopted from Breton et al. (2013).

	Sample		$^{87}Sr/^{86}Sr$	2se		$^{143}Nd/^{144}Nd$	2se		$^{206}Pb/^{204}Pb$	2se	$^{207}Pb/^{204}Pb$	2se	$^{208}Pb/^{204}Pb$	2se
	CT02-373		0.705277	0.000015		0.512609	0.000006		18.4535	0.0008	15.5631	0.0007	39.0977	0.0016
	CT02-598		0.705207	0.000013		0.512615	0.000005		18.4450	0.0008	15.5513	0.0007	39.0633	0.0018
	EF92-18		0.705255	0.000008		0.512613	0.000006		18.5839	0.0006	15.5797	0.0005	39.2652	0.0015
	EF92-25		0.705200	0.000011		0.512635	0.000010		18.2765	0.0012	15.5541	0.0011	38.7831	0.0027
	LVLK-85		0.705200	0.000010		0.512624	0.000008		18.4032	0.0005	15.5546	0.0004	39.0021	0.0014
	OB93-525		0.705328	0.000012		0.512591	0.000005		18.4879	0.0004	15.5592	0.0003	39.1076	0.0009
	JB-3		0.703387	0.000007		0.513062	0.000003		18.2971	0.0005	15.5392	0.0004	38.2550	0.0011
	JB-3		0.703388	0.000010		0.513058	0.000005		18.2968	0.0004	15.5393	0.0004	38.2552	0.0011
	JB-3		0.703393	0.000014		0.513058	0.000004		18.2970	0.0003	15.5395	0.0003	38.2553	0.0008
Average *	JB-3		0.703384	(n=32)		0.513065	(n=23)		18.2966	(n=21)	15.5393		38.2551	
2s §			0.000024			0.000011			0.0013		0.0016		0.0045	
	Standard	NIST987	0.710214		JNDi-1	0.512117		NIST981	16.9424		15.5003		36.7266	

Table S3 Sr-Nd-Pb isotopic compositions of Kerguelen basalts measured in this study. Note: * The long-term average isotopic compositions of JB-3 were measured at Hokkaido University. § Typical analytical error for sample JB3.